



3D-printed device for synthesis of magnetic and metallic nanoparticles

Vini Singh¹

Received: 22 August 2020 / Accepted: 27 October 2020 / Published online: 16 November 2020
© Akadémiai Kiadó 2020

Abstract

A cost-effective biodegradable droplet-based 3D-printed device for synthesis of superparamagnetic iron oxide (magnetite, Fe_3O_4) and metallic (silver, Ag and gold, Au) nanoparticles is demonstrated. The device was successful in confining the reagents in droplets and allowing a sequential flow of droplets to obtain uniform shape and size of both magnetic and metallic nanoparticles, an important characteristic for biomedical and sensing applications. Translating a conventional macroscale glassware-based to a fluidic-based synthesis involved a simple optimization in flow rates of dispersed (aqueous solutions of reagents) and continuous (oil) phases to fine tune the shape and size of magnetic and metallic nanomaterials. TEM confirmed the Fe_3O_4 and Ag/Au nanoparticles to possess nanoplate and sphere-shaped morphology, respectively. Further, utilization of gravitational force allowed a hassle-free controlled synthesis of nanoparticles, without any clogging of channel walls.

Keywords 3D-printing · Droplet-based method · Magnetic nanoparticles · Metallic nanoparticles

Introduction

Magnetic iron-oxide nanoparticles (NPs) have attracted immense attention because of their widespread applications as contrast agents in magnetic resonance imaging (MRI), as ferrofluids in biomedical applications such as drug carriers, hyperthermia treatment, theranostics, biosensors and bioanalysis [1–3]. In a similar fashion, metallic NPs such as silver (Ag) and gold (Au) exhibit interesting size and shape-dependent physical and chemical properties as against their bulk counterparts. Tailored shape and size of these metallic NPs exhibit localized surface plasmon resonance (LSPR) effect, which leads to strong enhancement of electromagnetic radiation on the interface, and therefore have shown promising applications in photovoltaic technology, sensing, heterogeneous catalysis, optoelectronics and nanomedicine [4–11]. The control of shape and size of NPs during synthesis is critical and of paramount importance for their applications. Bulk wet-chemical synthesis methods have been widely used to prepare colloidal magnetic and metallic dispersions.

However, this method suffers from drawbacks such as poor control over reagent addition, mixing, reaction time, and temperature leading to synthesis of polydisperse nanomaterials with a wide particle size distribution. This method is non-reproducible from one batch to another and hence limits its scalability to larger production volumes. Therefore, to overcome these drawbacks an alternate synthesis method is needed that is capable of synthesizing monodisperse high-quality nanomaterials in good yield.

Microfluidic systems are robust tools that allow precise control of reaction conditions to yield products with narrow size distribution and reduced polydispersity. A milli fluidic co-axial flow device using capillaries was the first demonstration for synthesis of 7 nm sized spherical iron-oxide NPs with a maghemite ($\gamma\text{-Fe}_2\text{O}_3$) phase in microchannels [12]. Thereafter, a microfluidic device with 25 μm deep fluid channels patterned into polydimethylsiloxane (PDMS) using soft lithography was reported. Spinel-shaped 4 nm sized superparamagnetic Fe_3O_4 NPs using electrocoalescence were synthesized using a droplet-based approach where each microdroplet functioned as independent microreactor [13]. Mixing of reagents in single-phase microfluidic systems is diffusion-limited. On the contrary, droplet-based microreactors overcome this limitation by fast mixing of reagents, where reagents co-flow before droplet formation, in confined space with defined quantity of reagents [14–16]. Droplet-based

✉ Vini Singh
vini21jan@uohyd.ac.in

¹ School of Engineering Sciences and Technology, University of Hyderabad, Hyderabad 500046, India

microfluidics present inherent advantages such as low sample volume, control over heat and mass transport, no cross-contamination, and negligible channel fouling because of co-flow of immiscible liquid e.g., oil (continuous phase) with aqueous reagent solutions (dispersion phase) which wets the channel walls thereby preventing sample adsorption [17]. The capillary based droplet microreactor for synthesis of 3.6 nm sized Fe_3O_4 NPs was reported, where the experimental set-up required a heated oil bath for growth and crystallization of particles and the sample had slight traces of non-superparamagnetic $\alpha\text{-Fe}_2\text{O}_3$ (hematite) [18]. Continuous single-phase [19, 20], droplet-based [21–24] and both combined together [25] for the synthesis of uniform spherical/rod/star/cube shaped and size in the range 3.1–34.2 nm Ag and Au NPs have also been reported. However, these studies required either expensive organic based precursors or immiscible mineral oil, an oil bath for temperature control or expensive-cum-laborious PDMS soft lithography microfabrication clean-room facility. The present work therefore focused on the requirement of a minimal experimental set-up for synthesis of NPs by developing a simple miniaturized device by 3D-printing technology (fused filament fabrication, FFF) to overcome the time-consuming clean-room microfabrication steps.

FFF or fused deposition modelling (FDM) is one of the most popular and widely used 3D-printing technology over other types of 3D-printing technologies. The advantages the technique offers are cost-effectiveness in terms of printer cost and a wide range of readily available thermoplastic filaments such as acrylonitrile butadiene styrene (ABS), polystyrene (PS), polylactic acid (PLA), polycaprolactone (PCL) which can be used to print the object with good resolution. 3D-printing also called as additive manufacturing technology prints a 3D object from a digital file in a layer-by-layer fashion. The digital 3D object is basically designed using computer aided design (CAD) software and then saved as a 3D printer-readable file format for printing. The technique involves melting the filament by passing through a heated print head and building the object on a printing bed layer-by-layer [26, 27]. It is being widely used for prototyping in industrial, food, medical and pharmaceutical applications [28]. In the present work, our aim is to utilize 3D-printing technology to design and fabricate a droplet-based device which is easy to operate for the synthesis of magnetic as well as metallic NPs. Also, the vertical alignment of the device is to use the force of gravity to reduce the flow impedance within the channels of the device, and to obtain the droplets with negligible wall clogging. This type of 3D-printed vertical device is not reported in the literature. The device is useful for synthesis of magnetic as well as metallic NPs without any trace of other impurities at an ambient temperature. The NPs with good uniformity in shape and size are synthesized by this device by optimizing only the flow rates of dispersed and continuous phases.

Experimental

Reagents and materials Iron (II) chloride tetrahydrate ($\text{FeCl}_2 \cdot 4\text{H}_2\text{O}$) and octadecene were purchased from Alfa Aesar. Conc. hydrochloric acid (HCl) and sodium borohydride (NaBH_4) were from Molychem and S D Fine-Chem Ltd., respectively. Silver nitrate (AgNO_3), trisodium citrate ($\text{Na}_3\text{C}_6\text{H}_5\text{O}_7$), sodium hydroxide (NaOH), polysorbate 80 (Tween 80) were purchased from Sisco Research Laboratories Pvt. Ltd. Anhydrous chloroauric acid (HAuCl_4) and iron (III) chloride hexahydrate ($\text{FeCl}_3 \cdot 6\text{H}_2\text{O}$) were obtained from Alpha Chemika and LobaChemie, respectively. Disposable syringes were purchased from a local medical store. Syringe filters of pore size 0.22 μm were obtained from Moxcare Labware. PTFE tubing of inner diameter 0.8 mm was purchased from Sigma-Aldrich. Ultrapure water was used for sample preparation of desired concentrations.

Instrumentation The device was printed on a FABX 3D printer (ReddX Technologies Pvt. Ltd) by FFF process using a PLA filament. Syringe pumps (Model: BEAS II, GECOM India) were used in the experiments to deliver the reagent solutions in the device at different flow rates for the synthesis of nanomaterials. A UV-Vis-NIR spectrophotometer (Model: Cary 5000, Agilent Technologies) was used to record the absorbance spectra of the samples. X-Ray diffraction studies for identifying the lattice structure of the synthesized nanomaterials were performed on PANalytical (Model: XPert³ Powder, source: copper). Dynamic light scattering (DLS) measurements for analysing the hydrodynamic size of the nanomaterials were performed on a particle analyzer (Model: LitesizerTM 100, Anton Paar). The particle size, d-spacing and crystallinity of the materials were determined by transmission electron microscopy (TEM, Model: FEI Technai T20) operating at an accelerating voltage of 200 kV. The magnetic properties of magnetite NPs were measured by vibrating sample magnetometer (VSM, Lakeshore 665) and electron spin resonance (ESR) spectrometer (JEOL: JES-FA200).

Design of droplet-based 3D-printed device CAD software (Solidworks) was used to design the device. The easy-to-operate device has the dimensions 50 X 10 X 30 mm. The reactor was printed by FFF process utilizing a biodegradable PLA spool of thickness 1.75 mm. The printing speed was 50 mm/s. The channel width, depth and outlet diameter were kept uniform at 3 mm while the four inlets had a diameter of 2 mm for connecting to the syringe pumps via PTFE tubing. Fig. S1 shows the CAD model of the reactor with the dimensions. The nozzle size, layer height, shell thickness parameters were 0.4 mm, 30 mm and 10 mm, respectively, while the fill density parameter was set 100% in the Cura slicing software to obtain a complete infilling in the device. The device was

Table 1 Flow rates employed for the synthesis of NPs

Reagents Sample number	FeCl ₂ .4H ₂ O + FeCl ₃ .6H ₂ O + Tween 80: NaOH: Oil	AgNO ₃ ; Sodium citrate: Oil	HAuCl ₄ : NaBH ₄ + Sodium citrate: Oil
Sample 1	30: 30: 60 (ml/h)	30: 30: 60 (ml/h)	30: 30: 60 (ml/h)
Sample 2	20: 20: 40 (ml/h)	20: 20: 40 (ml/h)	20: 20: 40 (ml/h)
Sample 3	10: 10: 20 (ml/h)	10: 10: 20 (ml/h)	10: 10: 20 (ml/h)
Sample 4	5: 5: 10 (ml/h)	5: 5: 10 (ml/h)	5: 5: 10 (ml/h)

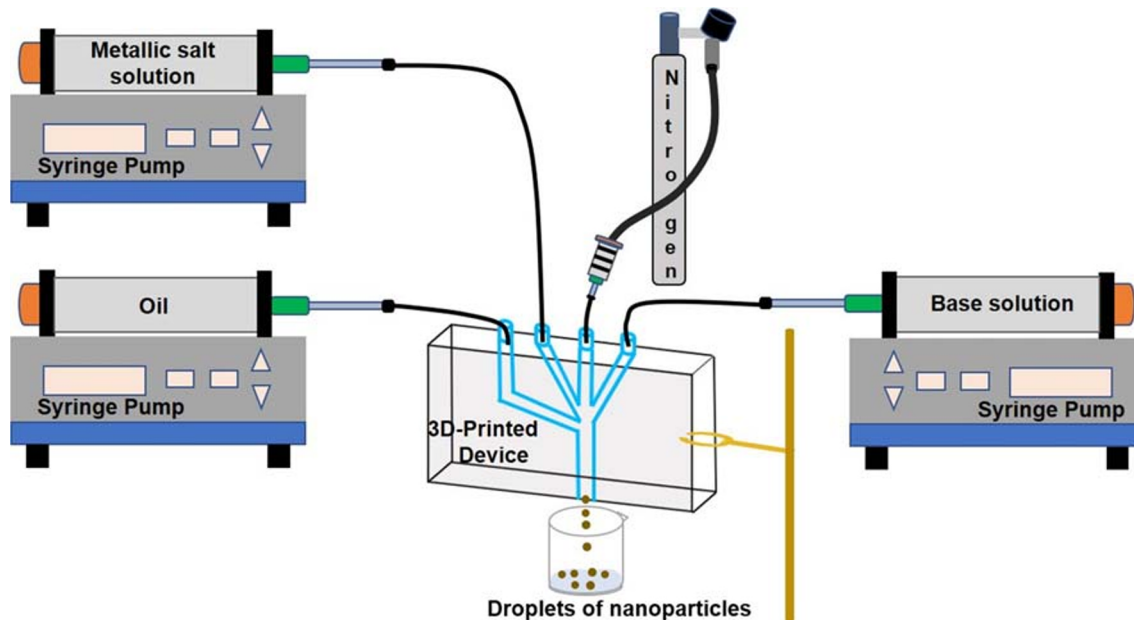
designed keeping the number of reagents and the reaction time in mind and also the minimum path the droplet needs to travel for immediate collection. Throughout the experiment the device stood vertical for the synthesis of magnetic and metallic NPs at room temperature.

Synthesis of magnetic iron-oxide (Fe₃O₄) NPs Iron salts in a molar ratio of 1FeCl₂.4H₂O: 2 FeCl₃.6H₂O (0.02 M, 0.04 M) and 0.05 M tween 80 in 0.4 M HCl, and 1.5 M NaOH were taken to synthesize Fe₃O₄ NPs. The synthesis was carried in an inert environment where one of the inlet of the device was used to purge nitrogen to prevent any intermediate or further oxidized products being formed in the reaction. The other three inlets served as the carriers for the flow of iron salts with tween 80 (mixed in a volumetric ratio of 1:1:1), reducing reagent NaOH, and octadecene as a continuous phase for droplet formation. These inlets were connected to the syringe pumps through PTFE tubing (outer diameter 1.6 mm), which controlled the flow rates of the reagent solutions for the synthesis. As shown in Fig. S1 the diameter of the inlets for

connecting the tubing was 2 mm, which was slightly more than the tubing outer diameter so that the tubing can be inserted in the device without any obstruction. There was no requirement for any nut and ferrule fittings for connecting the tubes with the device.

Synthesis of metallic silver (Ag) and gold (Au) NPs The synthesis of Ag NPs involved only two reagents; 1 mM AgNO₃ and 15 mM trisodium citrate. Trisodium citrate served as both reducing and stabilizing agent. The pH of the reducing agent was adjusted between 10 and 12 with 4.5 mM NaOH to facilitate enough supply of electrons for reducing Ag⁺ to Ag⁰. Three inlets of the device were used to pump AgNO₃, trisodium citrate and octadecene, connected to the syringe pumps through PTFE tubing, for synthesis of Ag NPs in droplets.

1 mM HAuCl₄ and 0.02 M NaBH₄ were the only reagents taken for the synthesis of Au NPs. Reducing agent NaBH₄ was mixed with 15 mM trisodium citrate in a volumetric ratio of 1:1 to stabilize the synthesized Au NPs. The experimental set-up was similar to the one used for synthesis of Ag NPs.

**Fig. 1** Schematic for synthesis of magnetic and metallic NPs at room temperature

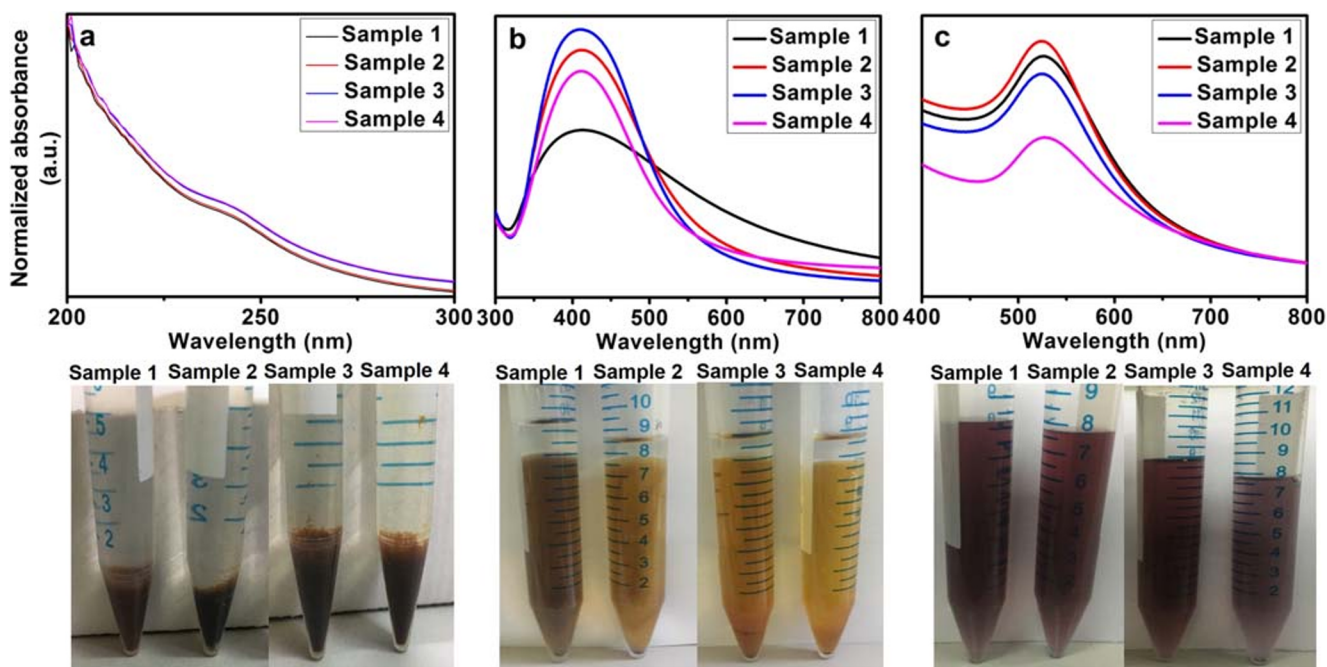


Fig. 2 UV-Vis absorbance spectrum of different samples of (a) Fe_3O_4 , (b) Ag and (c) Au NPs at room temperature

All the reagent solutions for the synthesis of both magnetic and metallic NPs were purged with nitrogen for 15 mins before the start of the experiment.

Figure 1 shows the schematic experimental set-up for the synthesis of NPs. The device is connected to the syringe pumps to flow the dispersed and the continuous phases at desired flow rates and kept vertical to allow a continuous synthesis of NPs in droplets. Fig. S2 shows the actual experimental setup.

Results and discussion

The flow ratio (R) of oil (R_O) to aqueous (R_A) streams decides the droplet formation when R is below 2.5. Maintaining $R \approx 1$ leads to droplet formation in the dripping mode, where the aqueous stream breaks at a small distance downstream of the T-junction [23]. The synthesis therefore involved the collection of a series of sample solutions of magnetic and metallic NPs by maintaining $R \approx 1$; varying the flow rates of aqueous solutions (dispersed phase) and oil suspension (continuous phase) from 30 ml/h to 5 ml/h. Table 1 shows the numbered sample solutions with different flow rates.

UV-Vis characterization of samples The UV-Vis characterization of samples 1–4 of Fe_3O_4 NPs revealed a peak absorbance at 243 nm (Fig. 2(a)) while samples 1–4 of Ag and Au NPs gave a peak absorbance at 400 nm (Fig. 2(b)) and 525 nm (Fig. 2(c)), respectively. The shape of the absorbance spectra of samples 3 and 4 of Ag NPs (Fig. 2(b)) was more uniform (stable, brown solution) when compared to samples 1 and 2, which displayed much broader peaks implying agglomeration and polydispersity in NPs (grey solution). The absorbance spectra of sample 2 of Au NPs (wine red solution, Fig. 2(c)) displayed a higher peak intensity with slightly narrow band width when compared to other samples of Au NPs. This

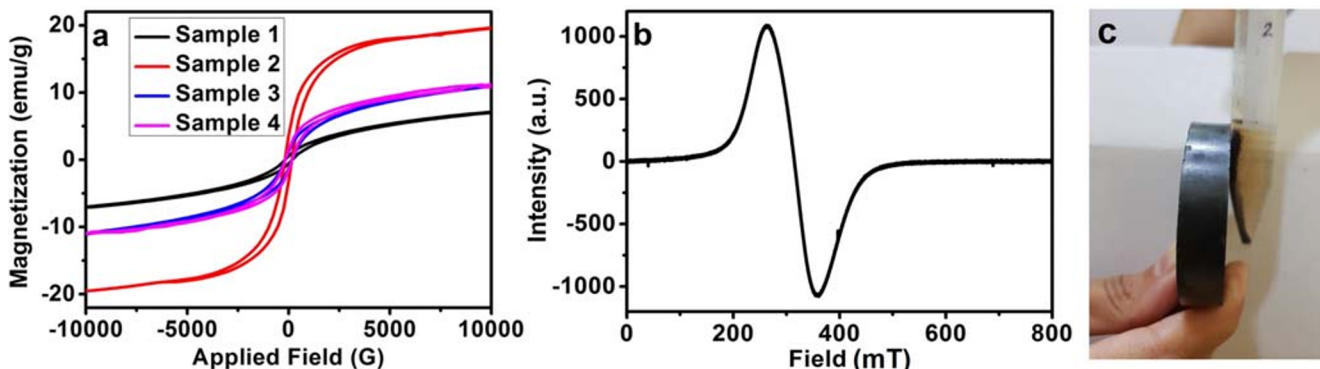


Fig. 3 a VSM, b ESR and c attraction of Fe_3O_4 NPs towards the magnet

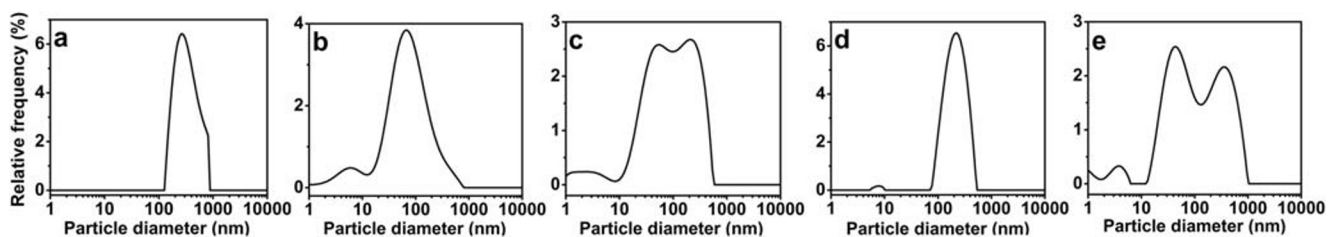


Fig. 4 Hydrodynamic size distribution of (a) sample 2 of Fe₃O₄, (b) sample 3 of Ag, (c) sample 4 of Ag, (d) sample 2 of Au and (e) sample 4 of Au NPs

indicates the formation of a higher concentration of similar shape and size of NPs. The absorbance peak of sample 4 of Au NPs (purple solution, Fig. 2(c)) was slightly broader which inferred either an agglomeration or formation of different shaped Au NPs. The ambiguity of this sample was however confirmed by DLS particle size measurements. The UV-Vis characterization however could not identify or confirm the best sample among the 4 samples of Fe₃O₄ NPs and hence magnetic measurements by VSM and ESR were carried.

VSM and ESR characterization of Fe₃O₄ NPs The magnetic properties of all the samples of Fe₃O₄ NPs were first characterized by VSM. The powdered samples of Fe₃O₄ NPs taken in teflon capsule exhibit a superparamagnetic behaviour, an important characteristic for biomedical applications, with a slight hysteresis in the magnetization curves (Fig. 3(a)). Among all the samples measured, sample 2 yielded a higher saturation magnetization ~20 emu/g at room temperature than the rest. This could infer incomplete reaction in sample 1 and high polydispersity in samples 3 and 4. Slightly low saturation magnetization in sample 2 could be either due to surface spin canting effect which reduces the electron spin-spin exchange/coupling among the Fe²⁺ and Fe³⁺ cations, or non-spherical shape of the nanoparticle or a dense non-magnetic surfactant which brings stoichiometric modifications on the nanoparticle surface [29, 30]. The ESR only on sample 2 taken in a quartz tube was performed to probe the magnetic anisotropy and gyromagnetic (*g*) factor of the nanomaterial. The ESR yielded a highly symmetric resonance spectra at room temperature (T = 295 K) with a *g* factor 2.13 confirming a homogeneous distribution of magnetic moment of NPs and

a narrow particle size distribution (Fig. 3(b)). *g* = 2.13 confirmed the superparamagnetic behaviour of the magnetic clusters aligned parallel to the applied field [31]. Low value of line width $\Delta H \sim 95$ mT implies the narrow size distribution of NPs. The superparamagnetic behaviour of the sample was also confirmed by the rapid attraction of the NPs towards the magnet in a span of roughly 15 s (Fig. 3(c)).

Hydrodynamic size and zeta potential measurements of Fe₃O₄, Ag and Au NPs The hydrodynamic sizes of the NPs were determined by DLS using ultrapure water as the dispersant. A intensity-weighted distribution measurement technique was used for estimating the particle size or specifically the hydrodynamic size distribution of NPs.

Large hydrodynamic size (413 ± 10 nm) of Fe₃O₄ NPs is due to the presence of dense surface coating of tween 80 (molecular weight: 1310 g/mol) to stabilize the NPs (Fig. 4(a)). Although tween 80 is a non-ionic surfactant, a negative zeta potential (-5 ± 1 mV) of NPs could probably infer the presence of ionic salts in the surfactant (Fig. 5(a)). In case of metallic NPs, the DLS measurements confirmed sample 3 of Ag NPs (hydrodynamic size 66 ± 4 nm) to have more uniformity in particle size (Fig. 4(b)) than sample 4 which appeared to be polydisperse (Fig. 4(c)). Similarly, sample 2 of Au NPs (hydrodynamic size 204 ± 14 nm) was better than sample 4 which gave a wide hydrodynamic size distribution (Fig. 4(d,e)). The synthesized Au NPs are comparatively larger in size than Ag NPs and the negative charge in Ag (-5 ± 2 mV) and Au (-13 ± 1 mV) NPs is because of the presence of coating of citrate ions on the particle surface (Fig. 5(b,c)). In addition to identifying the best samples among the synthesized NPs, the DLS measurements also confirmed that slow flow rates increased the

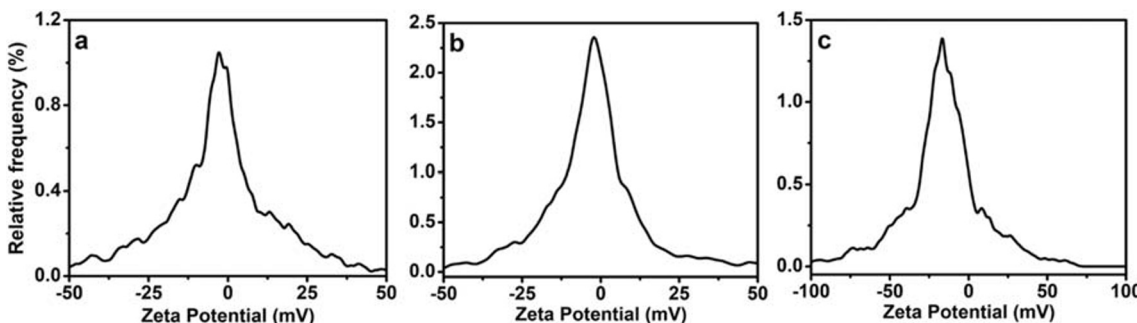


Fig. 5 Zeta potential of (a) sample 2 of Fe₃O₄, (b) sample 3 of Ag, and (c) sample 2 of Au NPs

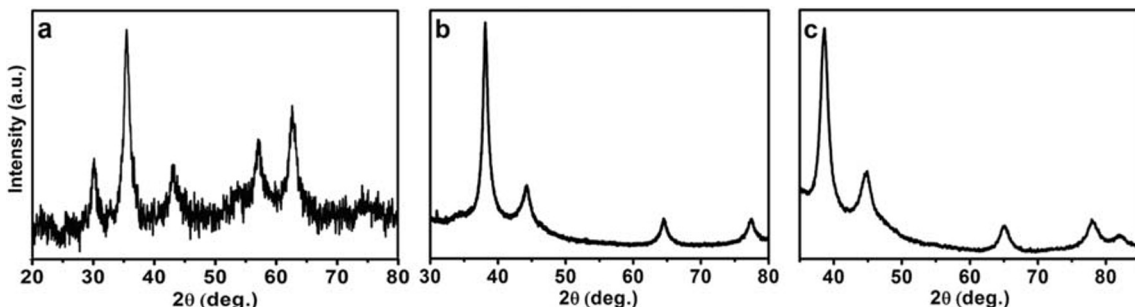


Fig. 6 XRD spectrum of (a) Fe₃O₄, (b) Ag, and (c) Au NPs at room temperature

polydispersity in NPs and thus slightly higher flow rates are to be employed to synthesize monodisperse NPs for the channel dimensions chosen for the device.

Furthermore, the flow patterns of sample 2 of Fe₃O₄ and Au, and sample 3 of Ag NPs were characterized by deducing the Reynolds number Re using the following equation $Re =$

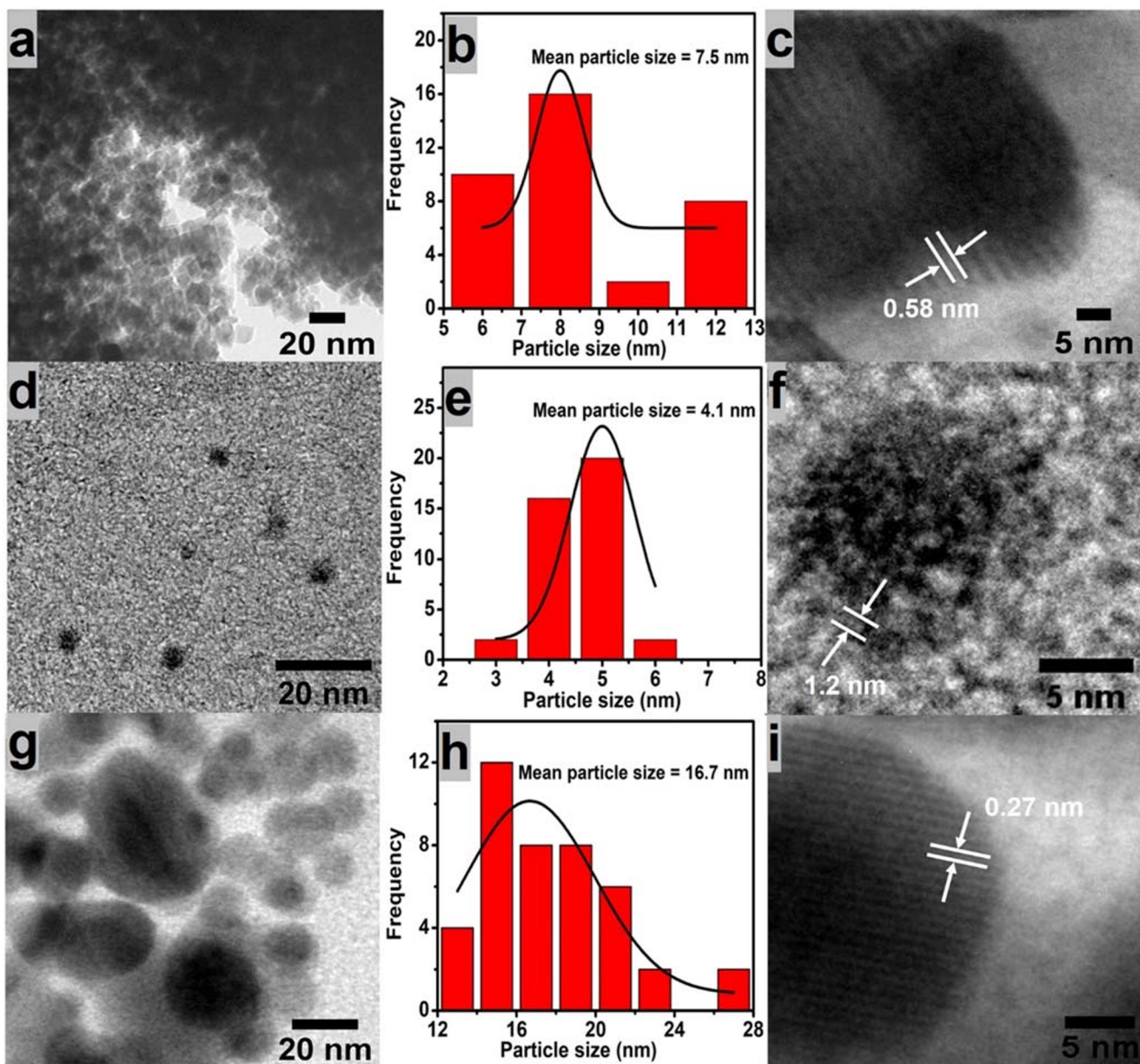


Fig. 7 TEM, histogram and HRTEM images of (a,b,c) Fe₃O₄, (d,e,f) Ag, and (g,h,i) Au NPs

$\frac{\mu D}{\nu}$ where, μ is the flow velocity of the fluid, D is the inner diameter of the channel, and ν is the kinematic viscosity of fluid (dynamic viscosity divided by density of fluid) [32]. In the present work, the flow velocity of the fluid was the combined flow rate of metallic salt and base solutions, and the kinematic viscosity was the viscosity of octadecene, used as the continuous phase (oil) in our experiment. Re for sample 2 of Fe_3O_4 and Au NPs was 1033 and for sample 3 of Ag NPs was 508. The obtained Re numbers were far lower than the critical value of 2100 indicating a laminar flow [33]. This justified the smooth vertical flow of NPs in the form of droplets under the force of gravity at high flow rates without any turbulence in the device.

XRD analysis of Fe_3O_4 , Ag and Au NPs The structural properties of the NPs were analysed by XRD. The XRD spectra of sample 2 of Fe_3O_4 , sample 3 of Ag and sample 2 of Au NPs were examined and their crystallite size was determined using Scherrer's formula $D_c = \frac{K\lambda}{b\cos\theta}$ where, D_c is the crystallite size of the nanomaterial, K is the Scherrer constant (varies with the shape of the crystal), λ is the X-ray wavelength (0.154 nm), b is the width of the diffraction peak at half maximum and θ is the Bragg angle of the reference peak [34]. Figure 6(a) shows the XRD spectra of Fe_3O_4 NPs which gave characteristic peaks at (220) (311) (400) (422) (511) (440) with no impurities at $2\theta = 30^\circ, 35^\circ, 43^\circ, 53^\circ, 57^\circ, 63^\circ$, respectively. The pattern matched well with JCPDS No. 82–1533 indicating a cubic crystal structure [35, 36]. The crystallite size calculated from the most intense peak (311) is ~ 7 nm. The XRD spectra of Ag NPs gave characteristic peaks at (111) (200) (220) (311) at $2\theta = 38^\circ, 44^\circ, 64^\circ, 77^\circ$, respectively, as shown in Fig. 6(b). The crystallite size calculated from the most intense peak (111) is ~ 5 nm. Figure 6(c) depicts the XRD spectra of Au NPs which gave characteristic peaks at (111) (200) (220) (311) (222) at $2\theta = 38^\circ, 44^\circ, 65^\circ, 78^\circ, 82^\circ$, respectively. The crystallite size calculated from the intense peak (111) is ~ 6 nm. The XRD patterns matched well with the standard pattern of Ag and Au NPs with JCPDS No. 04–0783 and 01–1174, respectively, both indicating a face-centered cubic crystal structure [37, 38].

TEM analysis of Fe_3O_4 , Ag and Au NPs The surface morphology of the droplet synthesized NPs was studied by TEM. Powdered form of sample 2 of magnetic Fe_3O_4 NPs was mixed with epoxy resin while liquid samples 3 and 2 of Ag and Au NPs, respectively were diluted in water and drop casted on carbon coated Cu grids for TEM analysis.

The Fe_3O_4 NPs were in clusters as they were embedded in an epoxy resin. They exhibited a regular shape with a nanoplate geometry and appeared to be of uniform size with a mean particle diameter $7.5 (\pm 2)$ nm (Fig. 7(a,b)). The NPs displayed a highly crystalline structure with a interplanar distance of $0.58 (\pm 0.12)$ nm (Fig. 7(c)). Ag and Au NPs also

exhibited uniformity in size and shape. Both the metallic NPs were isotropic with a spherical geometry. The size and interplanar distance of the Ag were $4.1 (\pm 1)$ nm (Fig. 7(d,e)) and $1.2 (\pm 0.1)$ nm (Fig. 7(f)), respectively, while the size and interplanar distance of Au NPs were $16.8 (\pm 3)$ nm (Fig. 7(g,h)) and $0.27 (\pm 0.04)$ nm (Fig. 7(i)), respectively. The particle sizes of Fe_3O_4 and Ag NPs matched well with the crystallite size estimated from XRD patterns with a standard deviation ± 1 nm while Au NPs were polycrystalline in nature. In addition, the TEM analysis also supported the low saturation magnetization of Fe_3O_4 NPs because of its non-spherical shape, and uniformity in shape and size as implied from ESR data.

Conclusions

The developed device is an attempt to demonstrate the synthesis of magnetic and metallic NPs in the form of droplets using 3D-printing technology. Each droplet functioned as a single reactor to obtain uniform nanoplatelet-shaped Fe_3O_4 and spherical-shaped Ag and Au NPs with a narrow size distribution. The utilization of force of gravity to synthesize the NPs was advantageous as it helped in reducing the impedance in fluid flow and also prevented fouling and channel blockage for a continuous synthesis of NPs. Indeed, a simple optimization in the flow rates of aqueous and oil streams for the synthesis of both magnetic and metallic NPs proved easy-to-operate functionality and versatility of the simple 3D-printed device.

Supplementary Information The online version contains supplementary material available at <https://doi.org/10.1007/s41981-020-00124-3>.

Acknowledgements The author acknowledges Department of Science and Technology (DST), Government of India for financial support (Project number: SR/WOS-A/ET-46/2018) under the Women Scientist Scheme to carry out this work. The author is also grateful to Prof. Rajender Singh, School of Physics, University of Hyderabad for his critical inputs on the manuscript.

Compliance with ethical standards

The author declare no competing financial interests.

References

1. Singh V, Krishnan S (2015) Voltammetric immunosensor assembled on carbon-pyrenyl nanostructures for clinical diagnosis of type of diabetes. *Anal Chem* 87:2648–2654
2. Singh V, Krishnan S (2018) Electrochemical and surface plasmon insulin assays on clinical samples. *Analyst* 143:1544–1555
3. Wu K, Su D, Liu J, Saha R, Wang J (2019) Magnetic nanoparticles in nanomedicine: a review of recent advances. *Nanotechnology* 30:502003

4. Aroca R (2006) Ed., Surface-enhanced vibrational spectroscopy; John Wiley & Sons: Chichester, U.K.
5. Daniel MC, Astruc D (2004) Gold nanoparticles: assembly, supramolecular chemistry, quantum-size-related properties, and applications toward biology, catalysis, and nanotechnology. *Chem Rev* 104:293–346
6. Talapin DV, Lee JS, Kovalenko MV, Shevchenko EV (2010) Prospects of colloidal nanocrystals for electronic and optoelectronic applications. *Chem Rev* 110:389–458
7. Shalaev VM (2007) Optical negative-index metamaterials. *Nat Photonics* 1:41–48
8. Hu M, Chen J, Li Z-Y, Au L, Hartland GV, Li X, Marqueze M, Xia Y (2006) Gold nanostructures: engineering their plasmonic properties for biomedical applications. *Chem Soc Rev* 35:1084–1094
9. Shipway AN, Katz E, Willner I (2000) Nanoparticle arrays on surfaces for electronic, optical, and sensor applications. *ChemPhysChem* 1:18–52
10. Somorjai GA, Borodko YG (2001) Research in nanosciences – great opportunity for catalysis science. *Catal Lett* 76:1–5
11. Graf C, van Blaaderen A (2002) Metallodielectric colloidal core–shell particles for photonic applications. *Langmuir* 18:524–534
12. Hassan AA, Sandre O, Cabuil V, Tabeling P (2008) Synthesis of iron oxide nanoparticles in a microfluidic device: preliminary results in a coaxial flow millichannel. *Chem Commun* 15:1783–1785
13. Frenz L, El Harrak A, Pauly M, Begin-Colin S, Griffiths AD, Baret JC (2008) Droplet-based microreactors for the synthesis of magnetic iron oxide nanoparticles. *Angew Chem Int Ed* 47:6817–6820
14. Song H, Tice JD, Ismagilov RF (2003) A microfluidic system for controlling reaction networks in time. *Angew. Chem.* 115:792–796. *Angew Chem Int Ed* 42:768–772
15. Sarrazin F, Prat L, Di Miceli N, Cristobal G, Link DR, Weitz DA (2007) Mixing characterization inside microdroplets engineered on a microcoalescer. *Chem Eng Sci* 62:1042–1048
16. Kelly BT, Baret J-C, Taly V, Griffiths AD (2007) Miniaturizing chemistry and biology in microdroplets. *Chem Commun* 18:1773–1788
17. Suea-Ngam A, Howes PD, Srisa-Art M, DeMello AJ (2019) Droplet microfluidics: from proof-of-concept to real-world utility? *Chem Commun* 55:9895–9903
18. Kumar K, Nightingale AM, Krishnadasan SH, Kamaly N, Wylenzinska-Arridge M, Zeissler K, Branford WR, Ware E, DeMello AJ, DeMello JC (2012) Direct synthesis of dextran-coated superparamagnetic iron oxide nanoparticles in a capillary-based droplet reactor. *J Mater Chem* 22:4704–4708
19. Lin XZ, Terepka AD, Yang H (2004) Synthesis of silver nanoparticles in a continuous flow tubular microreactor. *Nano Lett* 4:2227–2232
20. Baber R, Mazzei L, Thanh NTK, Gavriliidis A (2015) Synthesis of silver nanoparticles in a microfluidic coaxial flow reactor. *RSC Adv* 5:95585–95591
21. Xua L, Peng J, Yanc M, Zhang D, Shen AQ (2016) Droplet synthesis of silver nanoparticles by a microfluidic device. *Chem Eng Process* 102:186–193
22. Hong T, Lu A, Liu W, Chen C (2019) Microdroplet synthesis of silver nanoparticles with controlled sizes. *Micromachines* 10:274
23. Duraiswamy S, Khan SA (2009) Droplet-based microfluidic synthesis of anisotropic metal nanocrystals. *Small* 5:2828–2834
24. Abalde-Cela S, Taladriz-Blanco P, de Oliveira MG, Abell C (2018) Droplet microfluidics for the highly controlled synthesis of branched gold nanoparticles. *Sci Rep.* 8:2440
25. Thiele M, Soh JZE, Knauer A, Malsch D, Dtranik O, Müller R, Csáki A, Henkel T, Köhler JM, Fritzsche W (2016) Gold nanocubes – direct comparison of synthesis approaches reveals the need for a microfluidic synthesis setup for a high reproducibility. *Chem Eng J* 288:432–440
26. Pryor S (2014) Implementing a 3D printing service in an academic library. *J Libr Adm* 54:1–10
27. Belhabib S, Guessasma S (2017) Compression performance of hollow structures: from topology optimisation to design 3D printing. *Int J Mech Sci* 133:728–739
28. Tappa K, Jammalamadaka U (2018) Novel biomaterials used in medical 3D printing techniques. *J Funct Biomater* 9:17
29. Lu A-H, Salabas EL, Schueth F (2007) Magnetic nanoparticles: synthesis, protection, functionalization, and application. *Angew Chem Int Ed* 46:1222–1244
30. Kandasamy G, Maity D (2015) Recent advances in superparamagnetic iron oxide nanoparticles (SPIONs) for in vitro and in vivo cancer nanotheranostics. *Int J Pharm* 496:191–218
31. Mamanja JB, Gamarra LF, de Souza Brito GE (2014) Synthesis and characterization of Fe_3O_4 nanoparticles with perspectives in biomedical applications. *Mater Res* 17:542–549
32. Holman JP (1986) In *Heat transfer*. 6th edn. New York, McGraw-Hill
33. Menon SE (2015) Fluid flow in pipes, *Transmission pipeline calculations and simulations manual*. Gulf Professional Publishing, Oxford, pp 149–234
34. Massart R, Cabuil V (1987) Synthesis in an alkaline medium of colloidal magnetite: control of the yield and of the particle size. *J Phys Chem* 84:967
35. Itoh H, Sugimoto T (2003) Systematic control of size, shape, structure, and magnetic properties of uniform magnetite and maghemite particles. *J Colloid Interf Sci* 265:83–295
36. Voit W, Kim DK, Zapka W, Muhammed M, Rao KV (2001) Magnetic behavior of coated superparamagnetic iron oxide nanoparticles in ferrofluids. *Mater Res Soc* 676:781–786
37. Yang X, Du Y, Li D, Lv Z, Wang E (2011) One-step synthesized silver micro-dendrites used as novel separation mediums and their applications in multi-DNA analysis. *Chem Commun* 47:10581–10583
38. Luo X, Du L, Wen Z, Lv W, Zhao F, Jiang X, Peng Y, Sun YL, Li Y, Rao J (2015) Remarkably enhanced red–NIR broad spectral absorption via gold nanoparticles: applications for organic photo-sensitive diodes. *Nanoscale* 7:14422–14433

Publisher's note Springer Nature remains neutral with regard to jurisdictional claims in published maps and institutional affiliations.



Vini Singh obtained her PhD in Chemistry from Oklahoma State University-Stillwater, USA under the supervision of Dr. Sadagopan Krishnan. Her thesis work was on the development of electrochemical and surface plasmon based clinical biosensors for diagnosis of type of diabetes. She is presently working as a DST Women Scientist at School of Engineering Sciences and Technology, University of Hyderabad, India. Her research activity is on design and development of 3D-printed microfluidic devices for chemical synthesis and sensing applications.